

First Measurement of Dijet Angular Distributions in the TeV Regime and Searches for Quark Compositeness and Extra Dimensions

The DØ Collaboration
URL <http://www-d0.fnal.gov>
(Dated: July 26, 2008)

We present a measurement of dijet angular distributions in Run II of the Fermilab Tevatron collider. The measurement is based on the Run IIa dataset, corresponding to an integrated luminosity of $\approx 0.7 \text{ fb}^{-1}$ taken with the DØ detector. Normalized shapes of dijet angular distributions have been measured over a range of dijet masses, from 0.25 TeV to above 1.1 TeV. This is the first time in collider-based high energy physics that differential distributions of a scattering process have been measured at partonic center-of-mass energies above 1 TeV. The data are in good agreement with the predictions of perturbative QCD and are used to constrain the parameter space in new physics models including quark compositeness, large extra dimensions, and TeV^{-1} scale extra dimensions. In some cases we obtain the most stringent limits from a hadron collider. These exclusion limits do not depend on the unknown Higgs mass.

I. INTRODUCTION

Of all high p_T processes at a hadron collider, jet production is the process with the largest cross section. For any given integrated luminosity, therefore jet production has the highest reach in energy and, correspondingly, probes the shortest distance scales. Dijet production is therefore an ideal observable with unique abilities to test the standard model in previously unexplored regions and to search for signals predicted by new physics models. The angular distribution of dijets with respect to the beam direction is directly sensitive to the dynamics of the underlying reaction (see Fig. 1). While in quantum chromodynamics (QCD) this distribution shows small but noticeable deviations from Rutherford scattering, a distribution much more strongly peaked in the central region would be a sign of new physics processes not included in the Standard Model, e.g. quark compositeness [1–3], large spatial extra dimensions according to the model proposed by Arkani-Hamed, Dimopoulos and Dvali, (ADD LED) [4, 5], or TeV^{-1} scale extra dimensions (TeV^{-1} ED) [6–8]. These models are described in section III.

By analyzing only the shape of the dijet angular distributions, we greatly reduce experimental uncertainties (e.g. jet energy calibration, luminosity) and theoretical uncertainties due to the renormalization scale dependence and the parton density functions (PDFs). The shape of the dijet angular distribution, however, still carries almost the full sensitivity to the new physics models

Dijet angular distributions and the closely related ratio of dijet mass distributions in different rapidity regions have been measured in Run I of the Fermilab Tevatron Collider by the CDF and the $D\bar{O}$ collaborations and been used to set limits on quark compositeness [9, 10]. In similar analyses, angular distributions of di-electrons and di-photons have been used to constrain the ADD LED and the TeV^{-1} ED models.

In this note we present the first measurement of dijet angular distributions in $p\bar{p}$ collisions at a center-of-mass energy of $\sqrt{s} = 1.96 \text{ TeV}$. The data sample, collected with the D0 detector during 2004-2005 in Run II of the Fermilab Tevatron Collider, corresponds to an integrated luminosity of $\mathcal{L} \approx 0.7 \text{ fb}^{-1}$. We measure distributions in the dijet variables $\chi_{\text{dijet}} = \exp(|y_1 - y_2|)$ and $y_{\text{boost}} = \frac{1}{2}|y_1 + y_2|$ in ten regions of dijet mass M_{jj} .

The rapidities y_1, y_2 of the two leading p_T jets in an event are closely related to the polar jet scattering angles by $y = \frac{1}{2} \ln \frac{1+\beta \cos \theta}{1-\beta \cos \theta}$ with $\beta = \frac{|\vec{p}|}{E}$. In the limit of massless $2 \rightarrow 2$ scattering processes, the variable χ_{dijet} is directly related to the polar scattering angle θ^* in the partonic center-of-mass frame by $\chi_{\text{dijet}} = \frac{1+\cos \theta^*}{1-\cos \theta^*}$. The χ_{dijet} distribution is therefore directly sensitive to the dynamics of the interaction. The specific choice of the variable χ_{dijet} is motivated by the fact that it has a flat distribution for Rutherford scattering.

In the limit of massless $2 \rightarrow 2$ scattering processes, the variable y_{boost} is related to the ratio of the momenta of the incoming partons by $y_{\text{boost}} = \frac{1}{2} \ln \left(\frac{x_{\text{max}}}{x_{\text{min}}} \right)$. Therefore the y_{boost} distribution reflects the imbalance in the proton momentum fractions x carried by the partons which enter the hard subprocess.

The phase space of this analysis is defined by $M_{\text{jj}} > 0.25 \text{ TeV}$, $\chi_{\text{dijet}} < 16$, and $y_{\text{boost}} < 1$ (see Figs. 2 and 3). The χ_{dijet} and y_{boost} requirements restrict the jet phase space to $|y_{\text{jet}}| < 2.4$ (see Fig. 3) where jets are well reconstructed in the $D\bar{O}$ detector and the calibration is known to high precision. The distributions of χ_{dijet} and y_{boost} in the different M_{jj} ranges are normalized by their respective integrals. Based on the χ_{dijet} measurement we set limits on quark compositeness, ADD large extra dimensions, and TeV^{-1} extra dimensions, some of which are the most stringent limits from a hadron collider. In contrast to the results from electroweak fits, our exclusion limits on different extra dimension models are independent of the unknown mass of the Higgs boson.

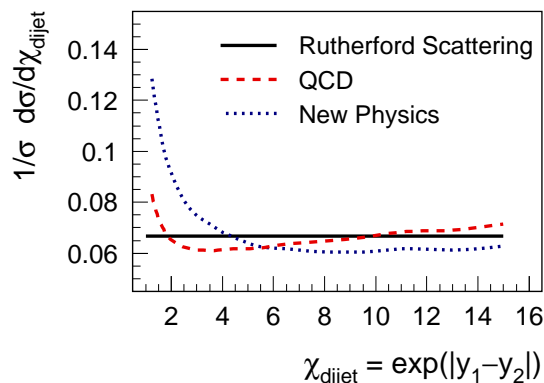


FIG. 1: The dijet angular distribution as a function of the variable χ_{dijet} (see text) for Rutherford scattering (solid line), QCD (dashed line), and for new physics models (dotted line). Details on the observable and the new physics models are described in the text.

II. MEASUREMENT

A detailed description of the DØ detector has been given elsewhere [11]. The event selection, jet reconstruction, jet energy and momentum correction in this measurement follow closely those used in our recent measurement of the inclusive jet cross section [12]. The primary tool for jet detection is the finely segmented uranium-liquid argon calorimeter that has almost complete solid angular coverage $1.7^\circ \lesssim \theta \lesssim 178.3^\circ$ [11]. Jets are defined by the Run II midpoint cone jet algorithm [13] with cone half opening angle of $R = 0.7$ in y and azimuthal angle. The same algorithm is used consistently in the experiment and in all theory calculations. Events are triggered by the jet with highest p_T in an event (p_T^{max}). To each M_{jj} region we assign a single trigger such that the smallest accessible p_T^{max} is above the trigger p_T threshold. The M_{jj} regions utilize triggers with different prescales, resulting in the following integrated luminosities 0.0987 pb^{-1} ($0.25 > M_{jj} > 0.4 \text{ TeV}$), 1.54 pb^{-1} ($0.4 > M_{jj} > 0.5 \text{ TeV}$), 17.2 pb^{-1} ($0.5 > M_{jj} > 0.6 \text{ TeV}$), 73.0 pb^{-1} ($0.6 > M_{jj} > 0.8 \text{ TeV}$), 508 pb^{-1} ($0.8 > M_{jj} > 1.0 \text{ TeV}$), and 707 pb^{-1} ($M_{jj} > 1.0 \text{ TeV}$).

The jet four-vectors are corrected for the response of the calorimeter, instrumental energy showering in and out of the jet cone, and additional energy from event pile-up and multiple $p\bar{p}$ interactions [12]. In addition, systematic shifts in $|y|$ due to detector effects are also corrected. The position of the $p\bar{p}$ interaction is reconstructed using a tracking system consisting of silicon microstrip detectors and scintillating fibers, located inside a solenoidal magnetic field of 2 T [11]. The position of the vertex along the beamline is required to be within 50 cm of the detector center. To suppress cosmic ray background with a signal efficiency of $> 99.5\%$, the missing transverse momentum in an event is required to be $< 70\%$ of the uncorrected p_T^{max} for uncorrected $p_T^{\text{max}} < 100 \text{ GeV}$ and $< 50\%$ of the uncorrected p_T^{max} for uncorrected $p_T^{\text{max}} > 100 \text{ GeV}$. Requirements on characteristics of shower development for genuine jets are used to suppress the remaining background due to electrons, photons, and detector noise that mimic jets. The efficiency for these requirements is above 97.5%. With these requirements, the fraction of background events is below 0.1% at all M_{jj} .

The data are corrected for instrumental effects, and the results are presented as dijet distributions at the “particle level” (according to [14]). Events, generated with PYTHIA v6.412 [15] with tune QW [16] and CTEQ6.5M PDFs [17], are reweighted according to the predictions from a perturbative QCD calculation in next-to-leading order (NLO) in the strong coupling constant using the same PDFs. These events are subjected to a fast simulation of the DØ detector response, based on parametrizations of resolution effects in p_T , the polar and azimuthal angle of jets, jet reconstruction efficiencies, and misidentification of the event vertex which have been determined from data and/or a detailed simulation of the DØ detector in Geant [18]. Based on the simulation, we obtain a rescaling function for the reconstructed M_{jj} that optimizes its correlation to the true particle level value. This increases the purity, the fraction of events with reconstructed M_{jj} values in a given M_{jj} bin that have true values in the same bin, in the different dijet mass regions to values between 45% and 70%. Applying the M_{jj} rescaling both to data and the simulation, we then use the simulation to determine bin-by-bin correction factors for the differential cross sections in χ_{dijet} and y_{boost} in the ten M_{jj} regions. These also include corrections for the energies of muons and neutrinos inside the jets that are not reconstructed. The total corrections for the differential cross sections are typically between 0.9 and 1.0, and never lower (larger) than 0.7 (1.1). The corrected differential cross sections within each M_{jj} range are subsequently normalized to their integrals, providing the corrected, final results for $\frac{1}{\sigma} \frac{d\sigma}{d\chi_{\text{dijet}}}$ and $\frac{1}{\sigma} \frac{d\sigma}{dy_{\text{boost}}}$.

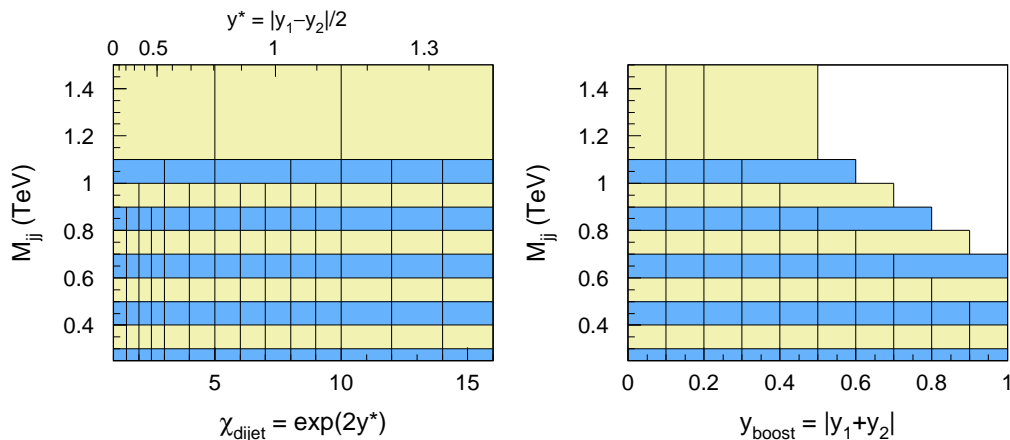


FIG. 2: The analysis phase space (shaded regions) in the plane of dijet mass and χ_{dijet} (left) and dijet mass and y_{boost} (right). The analysis bins are indicated by the lines. The white area is kinematically not accessible.

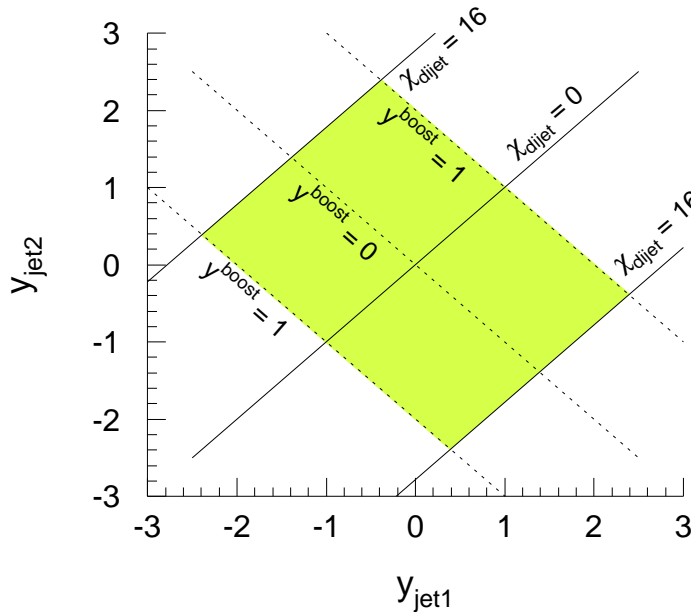


FIG. 3: The analysis phase space in the plane of the two jet rapidities y_1 and y_2 . The solid (dotted) lines connect points of identical χ_{dijet} (y_{boost}).

Correct statistical treatment of the data requires detailed knowledge of the correlations between uncertainties. Therefore the experimental systematic uncertainties have been split into single sources that are independent of each other, while the effects of each single source are fully correlated between all data points. Uncertainties due to the following sources of experimental uncertainties are determined using the simulation: jet energy calibration (49 sources), jet p_T resolution (15 sources), jet θ and ϕ resolution (3 sources each), systematic shifts in y (3 sources), jet reconstruction efficiency (3 sources), modeling of the vertex position, vertex misidentification and the uncertainty in the M_{jj} reweighting of the simulated events.

In the normalized distributions, many systematic uncertainties cancel to a large extent. The dominant uncertainties are due to the jet p_T resolution, and the jet energy calibration uncertainty. Smaller contributions are due to the uncertainties in the θ resolution and the systematic shifts in y . All other sources are negligible. For $M_{\text{jj}} < 1$ TeV, systematic uncertainties range between 1% – 5% and 3%–11% for $M_{\text{jj}} > 1$ TeV; they are in all cases much lower than the statistical errors.

The results are displayed in Fig. 4. The normalized χ_{dijet} and y_{boost} distributions are presented in ten M_{jj} regions, starting from $M_{\text{jj}} > 0.25$ TeV, and including one region for $M_{\text{jj}} > 1.1$ TeV. The statistical errors are indicated by the inner error bars, and the quadratic sum of statistical and systematic uncertainties is shown as the total error bar (the latter are hardly visible, since the systematic uncertainties are much smaller than the statistical errors). One can see that the χ_{dijet} distributions have almost no M_{jj} dependence. The y_{boost} distributions have a strong M_{jj} dependence, and are more strongly peaked towards $y_{\text{boost}} = 0$ at high M_{jj} . This is a direct consequence of the steeply falling PDFs for $x \rightarrow 1$.

The data are compared to theoretical predictions in next-to-leading order (NLO) in the strong coupling constant with non-perturbative corrections applied. The non-perturbative corrections are defined as the product of the corrections due to hadronization and the underlying event. These have been determined using PYTHIA v6.412 with tune QW and CTEQ6.5 PDFs. The PYTHIA cross sections have been reweighted in M_{jj} to agree with the NLO calculation. The NLO calculations are performed using fastNLO [19] based on NLOJET++ [20, 21]. Renormalization and factorization scales are varied together around the central value of $\mu = \langle p_T \rangle$ in the range $0.5 \leq \mu / \langle p_T \rangle \leq 2$, where $\langle p_T \rangle$ is the average dijet p_T . The calculations use the CTEQ6.6M PDFs [22] and their uncertainties as provided by the up and down variations of the 22 CTEQ6.6 uncertainty eigenvectors. The quadratic sum of scale and PDF uncertainties is displayed as a band around the central value. Both the scale and PDF uncertainties are, however, very small for these normalized distributions, so the band is nearly a line in Fig. 4. The theory, including the perturbative results and the non-perturbative corrections, is in good agreement with the data for both χ_{dijet} and y_{boost} over the whole M_{jj} range. For the χ_{dijet} distributions we have a χ^2 (see next section) of $\chi^2 = 124.9$ between theory and data (for 120 data points). Since there is no indication for any dynamics different from QCD, we proceed to set limits on new physics models.

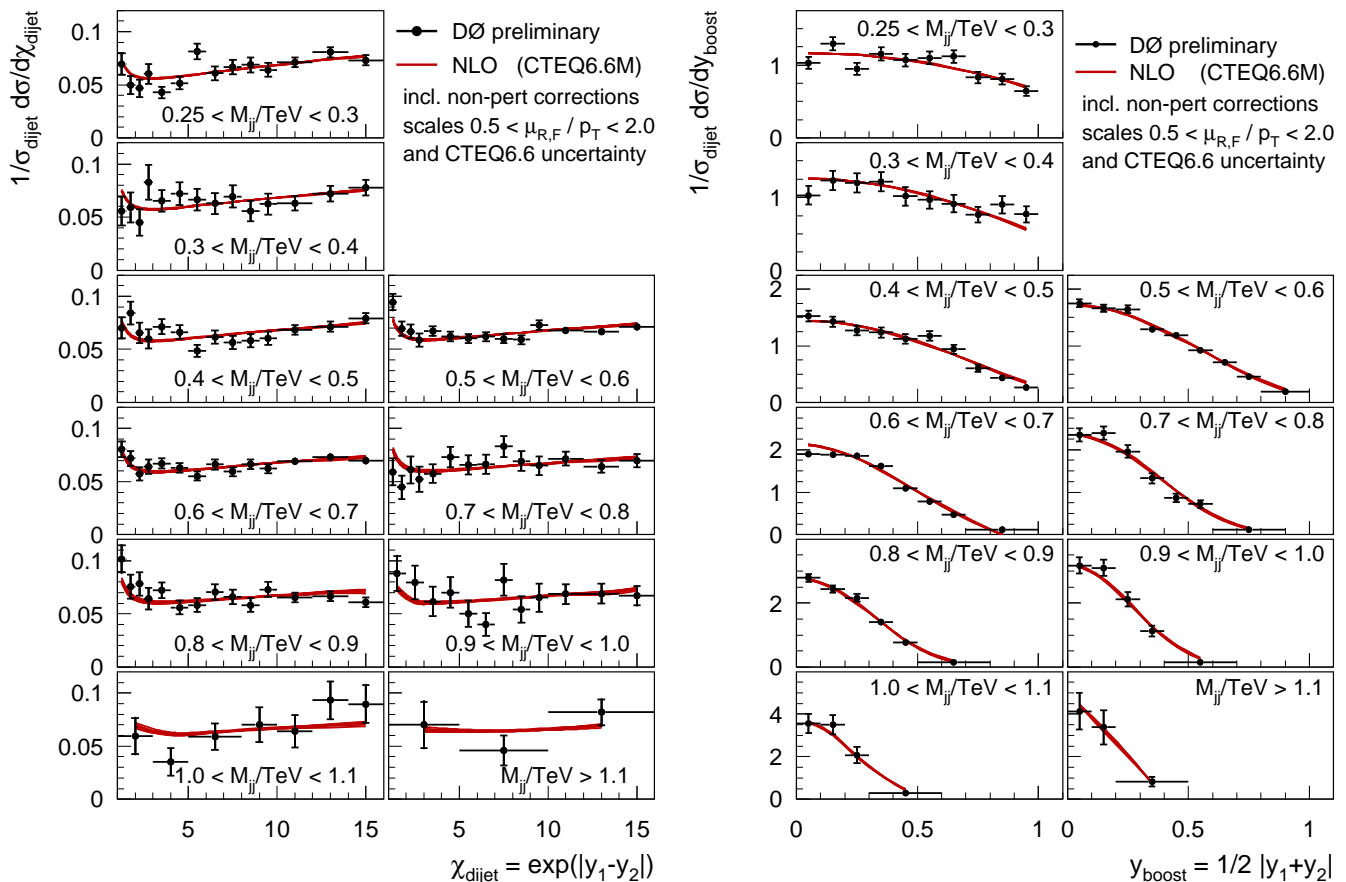


FIG. 4: The results for χ_{dijet} and y_{boost} vs. QCD. The statistical uncertainties are represented by the inner error bars and the total error bars correspond to the quadratic sum of statistical and systematic uncertainties (the latter are hardly visible since the systematic uncertainties are much smaller than the statistical errors). The theory band includes uncertainties from scale variations in the range $0.5 < \mu/\langle p_T \rangle < 2$ and the CTEQ6.6 PDF uncertainties.

III. INTERPRETATION: NEW PHYSICS LIMITS

Based on the agreement of the χ_{dijet} measurement with the Standard Model, we set limits on quark compositeness, ADD large extra dimensions, and TeV^{-1} extra dimensions models. In this section we describe the limit-setting procedure and give the results.

1. New Physics Models

a. Quark Compositeness Symmetries in groups of “particles” like atoms or hadrons have often been explained by substructure. Hypothetically quarks also could be made of other particles, as described in [1–3]. In this analysis we investigate the model in which all quarks are considered to be composite and we use the matrix elements from Ref. [2, 3]. The parameters in this model are the energy scale Λ and the sign of the interference term λ between the standard model and the new physics terms. Previous 95% CL quark compositeness limits are $\Lambda > 2.7 \text{ TeV}$ ($\lambda = +1$), $\Lambda > 2.4 \text{ TeV}$ ($\lambda = -1$), determined by DØ in Run I [10] from the ratio of dijet mass distributions at different angles (all quarks were assumed to be composite). The Run I measurements of the normalized χ_{dijet} distribution resulted in limits of $\Lambda^+ > 1.8 \text{ TeV}$ ($\lambda = +1$), $\Lambda^- > 1.6 \text{ TeV}$ ($\lambda = -1$) by CDF [9] and $\Lambda^\pm > 2.0 \text{ TeV}$ ($\lambda = \pm 1$) by DØ [10].

b. ADD-Large Extra Dimensions The “ADD large extra dimension” model [4, 5] assumes that extra dimensions exist in which gravity is allowed to propagate. The jet cross section receives additional contributions from virtual graviton exchange. The parameters in this model are the fundamental Planck scale M_S and, in one of three different formalisms (see below) also the number n of extra dimensions; and in another formalism the sign of the interference term λ . The re-analysis of the Run I dijet angular distributions from CDF [9] and DØ [10] has provided limits of $M_S >$

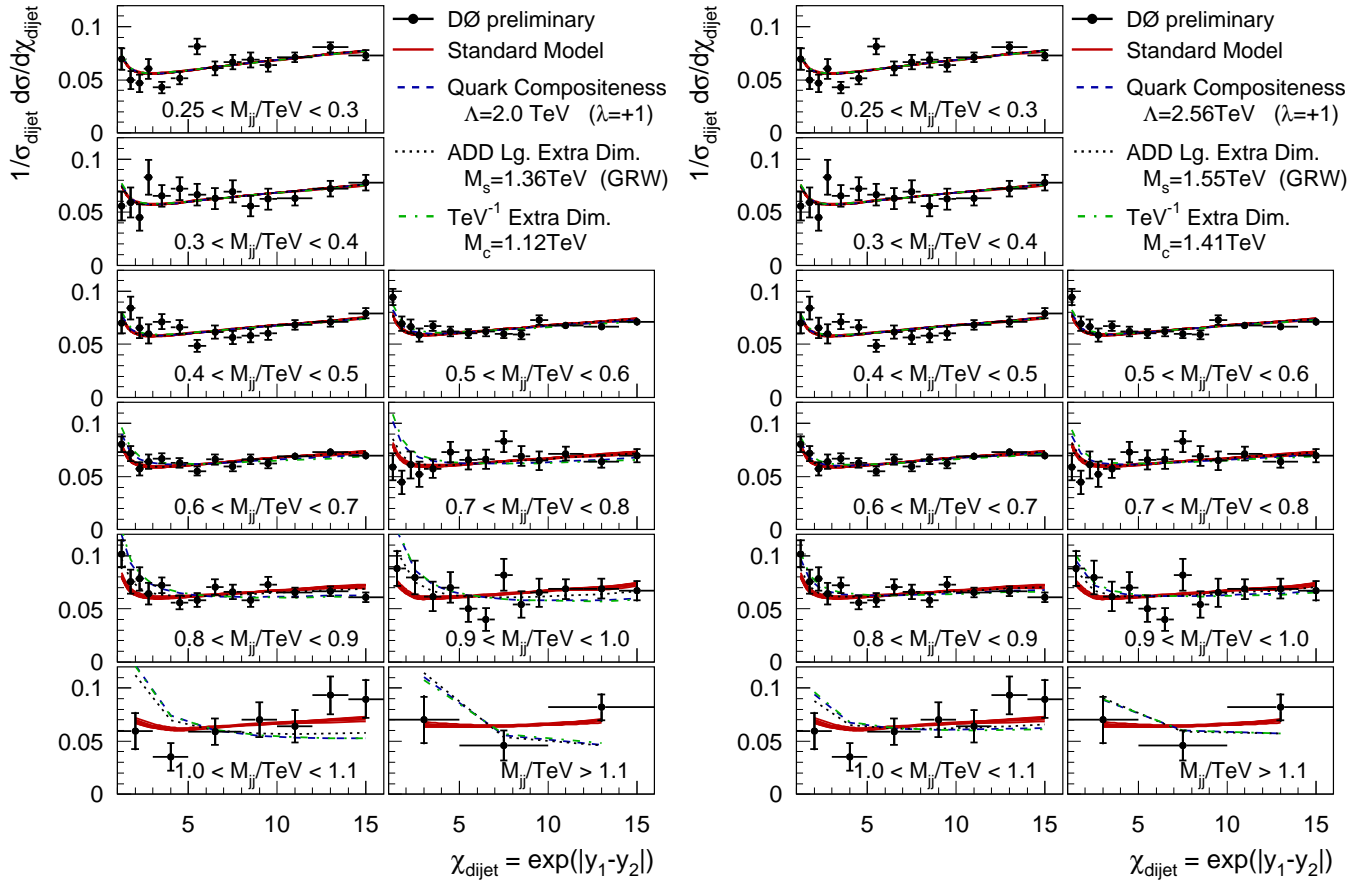


FIG. 5: The results for χ_{dijet} are compared to Standard Model predictions and to the predictions of various new physics models for lower (left) and higher mass scales (right). The statistical uncertainties are represented by the inner error bars and the total error bars correspond to the quadratic sum of statistical and systematic uncertainties (the latter are hardly visible since the systematic uncertainties are much smaller than the statistical errors). The Standard Model theory band includes uncertainties from scale variations in the range $0.5 < \mu/\langle p_T \rangle < 2$ and the CTEQ6.6 PDF uncertainties.

1.16 TeV [23]. The best limits from a single experiment come from $D\bar{O}$ in dielectron and diphoton production [24] and improved preliminary results have been presented in [25, 26]. The published (preliminary) 95% CL limit in the GRW formalism (see below) is $M_S = 1.2$ TeV (1.62 TeV). The matrix elements for our calculations are taken from Ref. [5].

c. TeV^{-1} Extra Dimensions The “ TeV^{-1} extra dimension” model [6–8] assumes that extra dimensions exist at the TeV^{-1} scale. Standard Model cross sections are modified due to the exchange of virtual Kaluza-Klein excitations of the SM gauge bosons, and not the graviton. In other words, gluons can travel through the extra dimensions, which changes the dijet cross section. The parameter in this model is the compactification scale M_C . So far, only a single limit on TeV^{-1} extra dimensions has been determined at the Tevatron. In a preliminary analysis of the dielectron mass spectrum [27] $D\bar{O}$ has set a 95%CL limit of $M_C = 1.12$ TeV. Higher sensitivity is achieved by the LEP experiments (the analysis in [8] finds a 95%CL limit of $M_C = 6.6$ TeV from the combined LEP data). We use the matrix elements from Ref. [8].

The cross sections for the new physics models consist of the standard model contribution f_{SM} and the model specific pieces f_{NP} (the “new physics” contribution) and f_{Int} (the interference term). All predictions have the form

$$\sigma_{\text{NP}} = f_{\text{SM}} + \eta \cdot f_{\text{Int}} + \eta^2 \cdot f_{\text{NP}}, \quad (1)$$

and the parameter η depends on the model

$$\begin{aligned} \text{Quark Compositeness:} & \quad \eta = \lambda/\Lambda^2, \\ \text{ADD-Large Extra Dimensions:} & \quad \eta = \mathcal{F}/M_S^4, \\ \text{TeV}^{-1} \text{ Extra Dimensions:} & \quad \eta = 1/M_C^2. \end{aligned} \quad (2)$$

In the ADD LED model different formalisms use different definitions for \mathcal{F}

$$\mathcal{F} = 1 \quad (\text{GRW}) [28], \quad (3)$$

$$\mathcal{F} = \begin{cases} \log(M_S^2/\hat{s}) & \text{for } n = 2 \\ 2/(n-2) & \text{for } n > 2 \end{cases} \quad (\text{HLZ}) [29], \quad (4)$$

$$\mathcal{F} = \frac{2\lambda}{\pi} = \pm \frac{2}{\pi} \quad (\text{Hewett}) [30], \quad (5)$$

and $\lambda = \pm 1$ is the sign of the interference term. The variable \hat{s} is the center of mass energy of the partonic subprocess which is at lowest order equal to M_{jj} . It is obvious that the results for GRW and HLZ agree for $n = 4$. The new physics contributions have only been calculated to LO, while the QCD predictions are known to NLO. In this analysis, to obtain the best estimate for new physics processes, we multiply the NLO QCD cross section with the LO correction factor for the new physics models. This procedure is equivalent to using the NLO corrections for the standard model predictions to rescale the LO predictions of the new physics models in each bin.

$$\sigma_{\text{NP}}^{\text{NLO}} = \sigma_{\text{QCD}}^{\text{NLO}} \cdot \frac{\sigma_{\text{NP}}^{\text{LO}}}{\sigma_{\text{QCD}}^{\text{LO}}} = \sigma_{\text{NP}}^{\text{LO}} \cdot \frac{\sigma_{\text{QCD}}^{\text{NLO}}}{\sigma_{\text{QCD}}^{\text{LO}}}. \quad (6)$$

This choice has also been used before in all similar related analyses [33]. The k-factors ($k = \sigma_{\text{QCD}}^{\text{NLO}}/\sigma_{\text{QCD}}^{\text{LO}}$) are in the range 1.25–1.5, increasing with M_{jj} and decreasing with χ_{dijet} . Their effects on single bins of the normalized χ_{dijet} distributions within the different M_{jj} regions is below 12%. The new physics cross sections are computed using the above-mentioned matrix elements [34]. It is important to note that all variations (the scale variations and the 22 CTEQ6.6 PDF uncertainty eigenvectors) are fully propagated into *all* of the three contributions $\sigma_{\text{QCD}}^{\text{NLO}}$, $\sigma_{\text{NP}}^{\text{LO}}$, and $\sigma_{\text{QCD}}^{\text{LO}}$. Therefore all of these pieces are computed throughout consistently with identical PDFs and renormalization and factorization scales.

Predictions for the different models are compared to the χ_{dijet} data and to the Standard Model results in Fig. 5 for smaller (left) and larger new physics mass scales (right). It is seen that all models predict increased contributions as $\chi_{\text{dijet}} \rightarrow 1$ towards large M_{jj} (the decrease for large χ_{dijet} is a consequence of the normalization). The M_{jj} evolution of the increase towards small χ_{dijet} is seen to be different for different models. The dependence of the models on their parameters can be seen in the comparison of the left and right Figures.

2. Limit Setting Procedure

We define the χ^2 between data and theory using the standard formula which introduces nuisance parameters for each systematic uncertainty which is correlated between different data points. This includes all single sources of experimental and theoretical uncertainties. The χ^2 is then minimized with respect to all nuisance parameters, and is therefore only a function of the new physics model parameter, referred to as ξ in the following. By computing $\chi^2(\xi)$ for different values of ξ we derive 95% CL limits on the latter. We use three different statistical approaches:

The first approach uses a “frequentist” definition in which the (single sided) 95% CL limit is defined by the value of ξ at which $\chi^2(\xi)$ has increased by $\chi^2(\xi) - \chi_{\text{min}}^2 = 3.84$ with respect to its minimum value [32]. The corresponding limits are labeled “frequentist limits”[35].

The second and third approaches use a Bayesian definition to define the 95% CL parameter limits. The $\chi^2(\xi)$ is transformed into a likelihood function defined as

$$L(\xi) = \frac{1}{A} \exp\left(-\frac{1}{2} \chi^2(\xi)\right) P(\xi). \quad (7)$$

In this formula A is the normalization (obtained from the requirement that the integral over $L(\xi)$ is unity) and $P(\xi)$ is the prior probability distribution of ξ . Since $\chi^2(\xi)$ is minimized with respect to all nuisance parameters, this is the “profiled likelihood”. We then compute the integral

$$Q(\xi) = \int_0^\xi L(\xi') d\xi', \quad (8)$$

as a function of ξ and obtain the one-sided 95% C.L. lower limit ξ_{limit} from

$$Q(\xi_{\text{limit}}) = 0.95 \cdot Q(\infty). \quad (9)$$

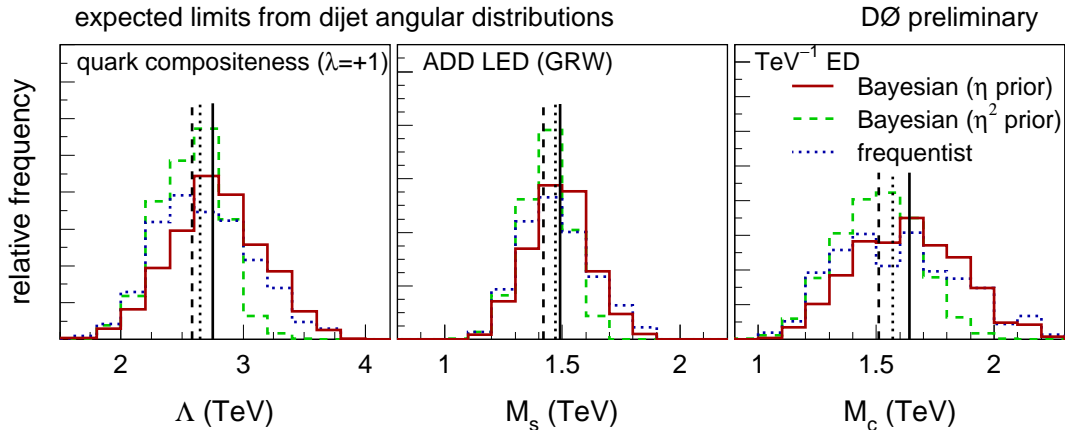


FIG. 6: The distributions of the expected limits for different new physics models and for different limit definitions. The vertical lines indicate the medians of the distributions.

This limit on ξ is then transformed back into the limit of the mass scale in the respective new physics model. The difference between the second and the third approach is the choice of the prior $P(\xi)$. In the second approach we choose $P(\xi)$ to be flat in the same power of the new physics mass scale by which it appears in the *Lagrangian* of the respective model. This corresponds to a prior that is flat in the variable η as defined in Eq. (1).

In the third approach we choose the prior $P(\xi)$ to be flat in the same power of the new physics mass scale by which it appears in the *cross section* of the respective model. In the notation of Eq. (1), this corresponds to a prior that is flat in the variable η^2 .

The feature in the second approach (Bayesian with prior flat in η) is that the prior, when translated into cross section, shows a considerable preference for zero as a result. This directly translates into a lower cross section limit for the same data and thus a higher parameter limit. This approach has, however, been used in many previous analyses which have derived limits on the new physics models under study [8, 24, 25, 27, 31]. In other cases [10] limits for both priors have been published. For direct comparisons with those previous results one should use the corresponding results from our analysis.

The expected 95% CL limits have been determined as the median values in 1000 pseudo-experiments generated based on the theoretical predictions, smeared according to the experimental and theoretical systematic uncertainties, and also smeared according to the expected statistical fluctuations. For each of the three approaches and for all models (and all different formalisms), we have determined the expected limits as the median of the distributions, together with the one sigma surrounding regions. The distributions are shown in Fig. 6. for the quark compositeness model for $\lambda = +1$ (left), the ADD LED model in the GRW formalism (center) and the TeV^{-1} ED model (right). The results for the different statistical approaches are presented using different linestyles, and the medians are indicated by vertical lines (in the corresponding linestyles). The limits for all three approaches are similar. As expected, the Bayesian approach with a prior flat in η produces stronger limits as compared to a prior flat in η^2 . The results for the frequentist approach are always in between the two Bayesian approaches. The distributions of χ^2 , the likelihood, and the probability (defined as the integrated likelihood) are shown in Fig. 7 for the different models.

For the ADD LED model χ^2 has the minimum at the standard model value ($M_S = \infty$) while for the quark compositeness model (for both signs of the interference term) χ^2 has a small minimum at $\Lambda = 5.14$ TeV with $\Delta\chi^2 = 0.02$ below the standard model value. Only for the TeV^{-1} ED model there is a slightly pronounced χ^2 minimum at $M_C = 2.17$ TeV with $\Delta\chi^2 = 0.72$ below the standard model value.

The complete results of the statistical analyses are presented in Table I. These include the expected limits (the median values), their surrounding one sigma regions as well as the limits determined from the data, for all models in all formalisms for the three statistical approaches. All experimental limits are close to the expected limits. The limits on the quark compositeness and TeV^{-1} ED models are slightly below the expected limits, whereas the experimental limits for the ADD LED model are slightly (by approximately half a standard deviation) above the expected limits. The limits in the Bayesian approach with prior flat in η are always largest, while the limits in the Bayesian approach with prior flat in cross section are smallest. The frequentist limits are always in between the two Bayesian results. Overall, the limits obtained using the frequentist and the different Bayesian approaches are very close and they always agree within 8% or better.

The limit on M_C in the TeV^{-1} ED model obtained in this analysis with $\approx 0.7 \text{ fb}^{-1}$ of data is a strong improvement, as compared to the previous preliminary result of $M_C > 1.12 \text{ TeV}$ in the dielectron channel with 200 pb^{-1} of data [27].

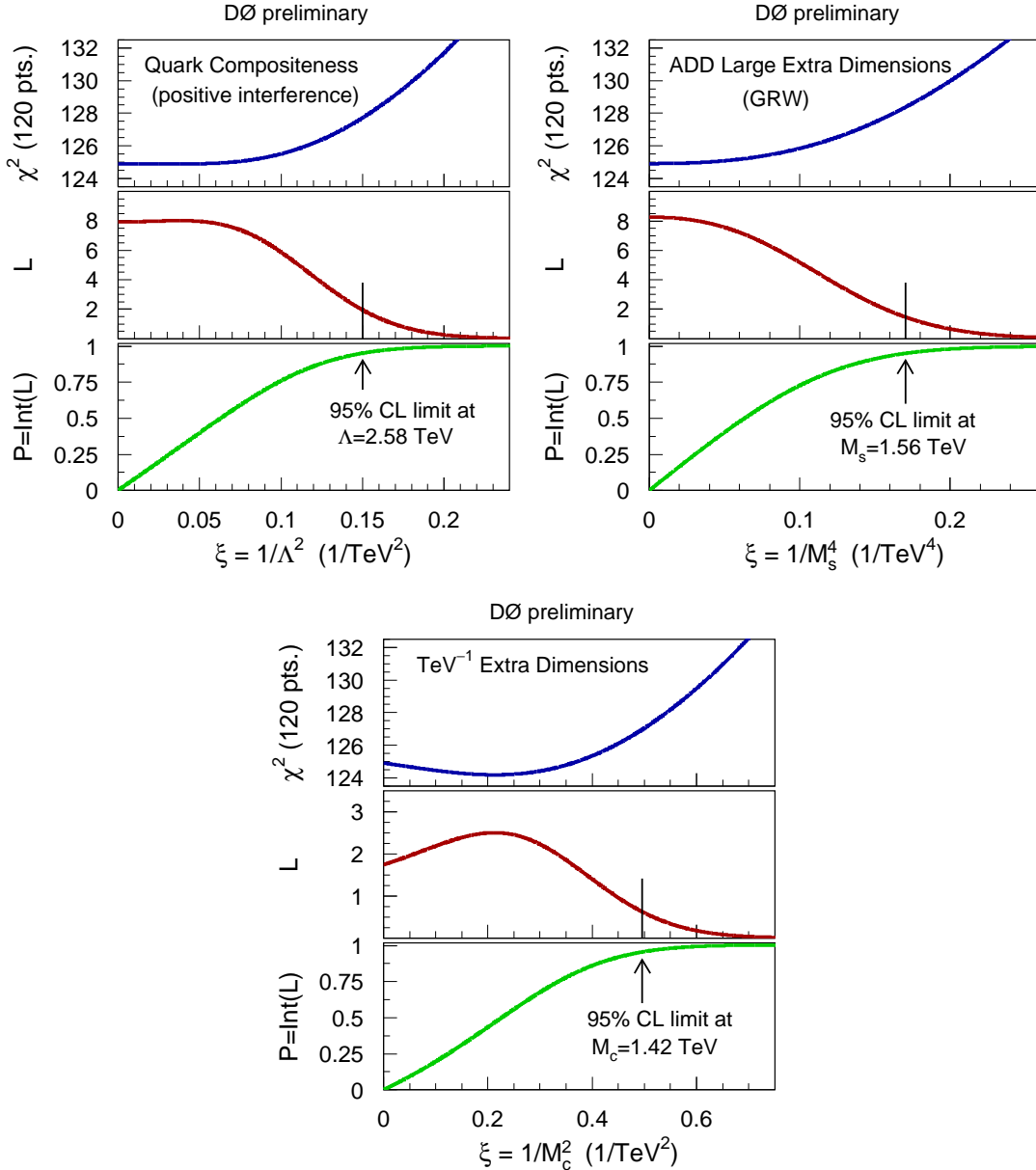


FIG. 7: The dependence of χ^2 (top), the likelihood (middle), and the probability (bottom) on the variable ξ which is directly related to the parameters of the new physics models. Indicated are the ξ values at which the probabilities has reached 95%, which defines the 95% CL limits on the parameters. The likelihoods and the probabilities are shown for the Bayesian procedure with prior flat in η (see text).

While the limits on M_S in the different formalisms of the ADD LED model are improving older results obtained from the combination of 200 pb^{-1} of dielectron and diphoton data [25], they are slightly lower as compared to the updated results from the combination of dielectron and diphoton data in Ref. [26], based on 1.05 fb^{-1} of data. Our result are, however, the most stringent limits from a single process at a hadron collider.

For the comparison of our limits on the quark compositeness model with the best existing limits, obtained from the ratio of dijet mass distributions in different angular regions [10], it must be considered that the latter results had been obtained in a Bayesian approach with prior flat in η , but for fixed PDFs and fixed scales in the theoretical calculations. If we derive our quark compositeness limits under the same assumptions, we obtain results of 2.73 TeV (2.64 TeV) for positive (negative) interference and these result are identical (superior), as compared to the results in [10]. If we compare the results for the preferred Bayesian approach with prior flat in η^2 , we improve the limits for both signs of the interference term (see Table XLIX in Ref. [10]).

DØ preliminary									
95% CL limits on New Physics models from the dijet angular distribution (in TeV)									
model (parameter)	χ^2 minimum		Bayesian				frequentist		previous limit
	position	depth	prior flat in η		prior flat in η^2		$\chi^2 - \chi^2_{\min} = 3.84$		
			expected	found	expected	found	expected	found	
Quark Composit. (Λ)									
$\lambda = +1$	5.10	0.02	2.75 ^{+0.43} _{-0.35}	2.58	2.58 ^{+0.28} _{-0.29}	2.39	2.65 ^{+0.42} _{-0.35}	2.46	2.73 [10]
$\lambda = -1$	5.22	0.02	2.78 ^{+0.36} _{-0.41}	2.54	2.55 ^{+0.31} _{-0.33}	2.35	2.65 ^{+0.45} _{-0.39}	2.42	2.49 [10]
TeV ⁻¹ ED (M_C)	2.17	0.66	1.64 ^{+0.23} _{-0.25}	1.42	1.51 ^{+0.16} _{-0.19}	1.33	1.57 ^{+0.33} _{-0.24}	1.35	1.12 [27]
ADD LED (M_S)									
GRW	∞		1.49 ^{+0.12} _{-0.14}	1.56	1.44 ^{+0.10} _{-0.10}	1.48	1.47 ^{+0.16} _{-0.14}	1.54	1.62 [26]
Hewett $\lambda = +1$	∞		1.33 ^{+0.11} _{-0.12}	1.39	1.28 ^{+0.09} _{-0.09}	1.32	1.31 ^{+0.14} _{-0.12}	1.37	1.22 [25]
Hewett $\lambda = -1$	∞		1.28 ^{+0.11} _{-0.09}	1.35	1.23 ^{+0.09} _{-0.08}	1.29	1.25 ^{+0.13} _{-0.09}	1.33	1.10 [25]
HLZ n=3	∞		1.77 ^{+0.14} _{-0.16}	1.85	1.71 ^{+0.11} _{-0.12}	1.76	1.74 ^{+0.19} _{-0.16}	1.83	1.94 [26]
HLZ n=4	∞		1.49 ^{+0.12} _{-0.14}	1.56	1.44 ^{+0.10} _{-0.10}	1.48	1.47 ^{+0.16} _{-0.14}	1.54	1.62 [26]
HLZ n=5	∞		1.35 ^{+0.11} _{-0.12}	1.41	1.30 ^{+0.09} _{-0.09}	1.34	1.32 ^{+0.14} _{-0.12}	1.39	1.46 [26]
HLZ n=6	∞		1.25 ^{+0.11} _{-0.10}	1.31	1.21 ^{+0.08} _{-0.09}	1.25	1.22 ^{+0.14} _{-0.11}	1.29	1.36 [26]
HLZ n=7	∞		1.19 ^{+0.09} _{-0.11}	1.24	1.14 ^{+0.08} _{-0.08}	1.18	1.17 ^{+0.13} _{-0.11}	1.22	1.29 [26]

TABLE I: The 95% CL exclusion limits on different New Physics models as obtained in this analysis (using Bayesian and frequentist methods), compared to the expected limits from this analysis and their one sigma band and to previous experimental limits. Also shown is the mass value for which a minimum in χ^2 was found, together with the χ^2 difference between the minimum and the Standard Model χ^2 .

3. Summary

We have presented the first measurement of dijet angular distributions in Run II of the Fermilab Tevatron collider, and the first measurement of angular distributions of a hard scattering process at partonic center of mass energies above 1 TeV in collider-based high energy physics. The normalized distributions in χ_{dijet} and y_{boost} are well described by theory calculations in next-to-leading order in the strong coupling constant. Based on the χ_{dijet} measurement we set limits on quark compositeness, ADD large extra dimension, and TeV⁻¹ extra dimension models. The results are presented using different Bayesian and frequentist approaches. For the quark compositeness model we obtain the most stringent limits to date. The limit on the TeV⁻¹ extra dimension model is the strongest limit from a hadron collider. The limits obtained on the ADD large extra dimension model are the most stringent limits from a single process at a hadron collider, and only slightly lower as compared to the combined limits from a recent analysis of dielectron and diphoton data.

Acknowledgments

We thank the staffs at Fermilab and collaborating institutions, and acknowledge support from the DOE and NSF (USA); CEA and CNRS/IN2P3 (France); FASI, Rosatom and RFBR (Russia); CAPES, CNPq, FAPERJ, FAPESP and FUNDUNESP (Brazil); DAE and DST (India); Colciencias (Colombia); CONACyT (Mexico); KRF and KOSEF (Korea); CONICET and UBACyT (Argentina); FOM (The Netherlands); PPARC (United Kingdom); MSMT (Czech Republic); CRC Program, CFI, NSERC and WestGrid Project (Canada); BMBF and DFG (Germany); SFI (Ireland); Research Corporation, Alexander von Humboldt Foundation, and the Marie Curie Program.

-
- [1] E. Eichten, I. Hinchliffe, K. D. Lane and C. Quigg, “Super Collider Physics,” Rev. Mod. Phys. **56**, 579 (1984) [Addendum-ibid. **58**, 1065 (1986)].
- [2] P. Chiappetta and M. Perrottet, “Possible bounds on compositeness from inclusive one jet production in large hadron colliders,” Phys. Lett. B **253**, 489 (1991).
- [3] K. D. Lane, “Electroweak and flavor dynamics at hadron colliders,” arXiv:hep-ph/9605257.
- [4] N. Arkani-Hamed, S. Dimopoulos and G. R. Dvali, “The hierarchy problem and new dimensions at a millimeter,” Phys. Lett. B **429**, 263 (1998) [arXiv:hep-ph/9803315].
- [5] D. Atwood, S. Bar-Shalom and A. Soni, “Dijet production at hadron colliders in theories with large extra dimensions,” Phys. Rev. D **62**, 056008 (2000) [arXiv:hep-ph/9911231].

- [6] K. R. Dienes, E. Dudas and T. Gherghetta, “Grand unification at intermediate mass scales through extra dimensions,” Nucl. Phys. B **537**, 47 (1999) [arXiv:hep-ph/9806292].
- [7] A. Pomarol and M. Quiros, “The standard model from extra dimensions,” Phys. Lett. B **438**, 255 (1998) [arXiv:hep-ph/9806263].
- [8] K. Cheung and G. Landsberg, “Kaluza-Klein states of the standard model gauge bosons: Constraints from high energy experiments,” Phys. Rev. D **65**, 076003 (2002) [arXiv:hep-ph/0110346].
- [9] F. Abe *et al.* [CDF Collaboration], “Measurement of dijet angular distributions at CDF,” Phys. Rev. Lett. **77**, 5336 (1996) [Erratum-ibid. **78**, 4307 (1997)] [arXiv:hep-ex/9609011].
- [10] B. Abbott *et al.* [D0 Collaboration], “High- p_T jets in $p\bar{p}$ collisions at $\sqrt{s} = 630$ GeV and 1800 GeV,” Phys. Rev. D **64**, 032003 (2001) [arXiv:hep-ex/0012046].
- [11] V.M. Abazov *et al.* (D0 Collaboration), Nucl. Instrum. Methods Phys. Res. A **565**, 463 (2006).
- [12] V. M. Abazov *et al.* [D0 Collaboration], “Measurement of the inclusive jet cross section in $p\bar{p}$ collisions at $\sqrt{s} = 1.96$ TeV,” arXiv:0802.2400 [hep-ex].
- [13] G.C. Blazey *et al.*, in *Proceedings of the Workshop: QCD and Weak Boson Physics in Run II*, edited by U. Baur, R.K. Ellis, and D. Zeppenfeld, Batavia, Illinois (2000) p. 47, See Section 3.5.
- [14] C. Buttar *et al.*, “Standard Model Handles and Candles Working Group: Tools and Jets Summary Report,” section 9, arXiv:0803.0678 [hep-ph].
- [15] T. Sjöstrand *et al.*, Comp. Phys. Comm. 135, 238 (2001).
- [16] T. Q. W. Group *et al.*, “Tevatron-for-LHC report of the QCD working group,” arXiv:hep-ph/0610012.
- [17] J. Pumplin *et al.*, JHEP **0207** (2002) 12; D. Stump *et al.*, JHEP **0310** (2003) 046.
- [18] Geant, Detector Description and Simulation Tool, CERN Program Library Long Writeup W5013
- [19] T. Kluge, K. Rabbertz and M. Wobisch, “fastNLO: Fast pQCD calculations for PDF fits,” arXiv:hep-ph/0609285.
- [20] Z. Nagy, “Next-to-leading order calculation of three-jet observables in hadron hadron collision,” Phys. Rev. D **68**, 094002 (2003) [arXiv:hep-ph/0307268].
- [21] Z. Nagy, “Three-jet cross sections in hadron hadron collisions at next-to-leading order,” Phys. Rev. Lett. **88**, 122003 (2002) [arXiv:hep-ph/0110315].
- [22] P. M. Nadolsky *et al.*, “Implications of CTEQ global analysis for collider observables,” arXiv:0802.0007 [hep-ph].
- [23] P. Mathews, S. Raychaudhuri and K. Sridhar, “Testing TeV scale quantum gravity using dijet production at the Tevatron,” JHEP **0007**, 008 (2000) [arXiv:hep-ph/9904232].
- [24] B. Abbott *et al.* [D0 Collaboration], “Search for large extra dimensions in dielectron and diphoton production,” Phys. Rev. Lett. **86**, 1156 (2001) [arXiv:hep-ex/0008065].
- [25] DØ preliminary di-electron and di-photon mass measurement, DØ conference note 4336, <http://www-d0.fnal.gov/Run2Physics/WWW/results/prelim/NP/N01/>
- [26] V. M. Abazov *et al.* [D0 Collaboration], “Search for large extra spatial dimensions in the dielectron and diphoton channels in pp-bar collisions at sqrt(s)=1.96 TeV”, preliminary result for ICHEP08.
- [27] DØ preliminary di-electron mass measurement, DØ conference note 4349, <http://www-d0.fnal.gov/Run2Physics/WWW/results/prelim/NP/N02/>
- [28] G. F. Giudice, R. Rattazzi and J. D. Wells, “Quantum gravity and extra dimensions at high-energy colliders,” Nucl. Phys. B **544**, 3 (1999) [arXiv:hep-ph/9811291].
- [29] T. Han, J. D. Lykken and R. J. Zhang, “On Kaluza-Klein states from large extra dimensions,” Phys. Rev. D **59**, 105006 (1999) [arXiv:hep-ph/9811350].
- [30] J. L. Hewett, “Indirect collider signals for extra dimensions,” Phys. Rev. Lett. **82**, 4765 (1999) [arXiv:hep-ph/9811356].
- [31] V. M. Abazov *et al.* [D0 Collaboration], “Search for large extra spatial dimensions in dimuon production at D0,” Phys. Rev. Lett. **95**, 161602 (2005) [arXiv:hep-ex/0506063].
- [32] W.-M. Yao *et al.*, “The Review of Particle Physics” Journal of Physics, G 33, 1 (2006) and 2007 partial update for 2008.
- [33] In some related analyses [9, 10], the k-factor ($k = \sigma_{\text{NLO}}/\sigma_{\text{LO}}$) was used which is equivalent to our procedure. In other analyses [24, 25, 27, 31], the LO calculation was normalized by a constant factor to agree with the data at low energies. In cases when this normalization factor agrees with the theoretical k-factor at low energies, and when the k-factor is not energy dependent, this approach is identical to the former approach. If the k-factor does have an energy dependence, however, the former approach is more consistent.
- [34] The private code for the calculations of the new physics model predictions has been tested in several ways: The LO Standard Model contributions from the new physics models have been compared with NLOJET++ and with PYTHIA. The results for the quark compositeness model have been compared with PYTHIA, and the TeV^{-1} ED model calculation was compared with the code used in [8]. In all cases we see perfect agreement.
- [35] A similar approach had been used in a previous analysis of dijet angular distributions [9], however, with a different criterion of $\chi^2 - \chi^2_{\text{Standard Model}} = 3.74$.